Pergamon

Acta Materialia 50 (2002) 883–899

Acta MATERIALIA

www.actamat-journals.com

# Strain energy distribution in ceramic-to-metal joints

J.-W. Park, P.F. Mendez, T.W. Eagar *

*Department of Materials Science and Engineering, Massachusetts Institute of Technology, Cambridge, MA 02139, USA*

Received 13 November 2000; received in revised form 24 September 2001; accepted 24 September 2001

**Abstract**

This work introduces a framework for evaluating the strength characteristics of ceramic-to-metal joints with multiple interlayers. Strain energy in the ceramic is used as a strength metric instead of maximum tensile stress. Based on the FEM analysis and order of magnitude scaling (OMS), simple analytical formulations between the strain energy and material properties are developed, which provide a guideline in designing multiple interlayers. Our analysis reveals the important role of multiple interlayers, which reduce the strain energy in the ceramic, increasing the strength of the joint. Based on the proposed design rule, $Si_3N_4$ to Inconel 718 joints have been brazed with single, double and triple interlayers and the joint strength was evaluated using a shear test. The experimental results support the design rules and confirm that strain energy is a good strength metric. 

*Keywords:* Ceramic-to-metal; Interlayer; Brazing; Strain energy

## 1. Introduction

Engineering ceramics possess fascinating properties as structural and electronic materials due to their excellent mechanical properties at high temperature as well as resistance to wear, erosion, oxidation and corrosion. As novel techniques for producing these materials have been developed, more and more interest has been focused on their use in advanced engineering designs [1]. There has been an increasing need for complex ceramic structures and ceramics have been incorporated into critical segments of overall structures. Reliable joining technologies are essential for full exploitation of the properties of the ceramic and for the success of the overall structure.

Significant differences in chemical and physical properties between ceramics and metals make it extremely difficult to find an effective joining process that maintains the strength and resilience of the joint. Two primary factors that inhibit formation of a mechanically reliable joint are the coefficient of thermal expansion (CTE) mismatch and the difference in the nature of the interatomic bond. On cooling from the joining temperature, residual stresses are induced due to the CTE mismatch and differing mechanical responses of the ceramic and the metal.

Generally, metals have a larger CTE and lower elastic modulus than the ceramic. In the joints analyzed in this study [Fig. 1(a)], large tensile and shear stresses are induced in the regions around the

* Corresponding author.
*E-mail address:* tweagar@mit.edu (T.W. Eagar).

1359-6454/02/$22.00 
PII: S1359-6454(01)00352-4

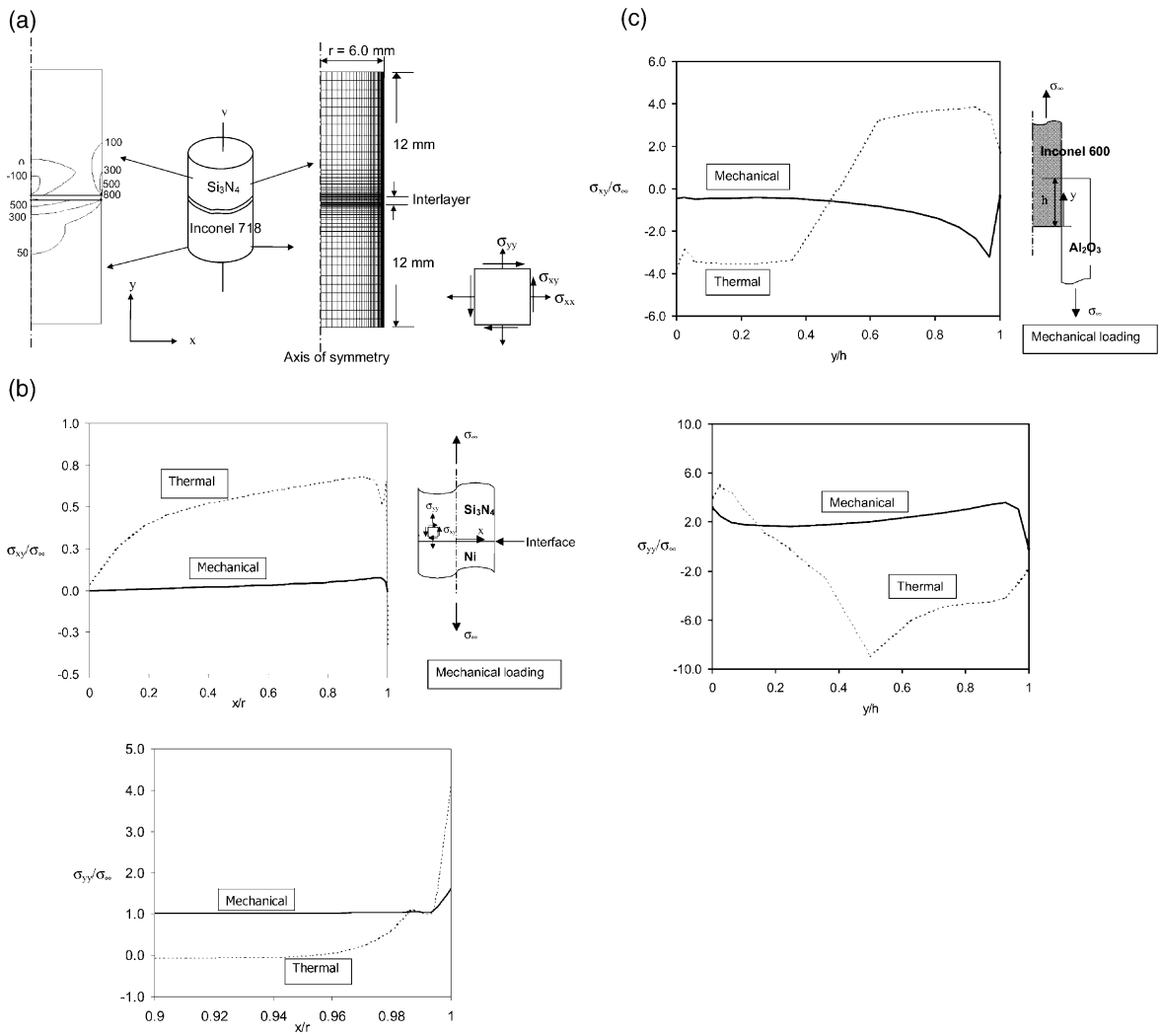


Fig. 1. (a) A schematic of the maximum principal stress distribution under thermal loading and FEM mesh configuration of a model joint. (b) A schematic of stress distributions in the ceramic near the interface along the *x*-direction of the model joint under mechanical or thermal loading. (c) A schematic of stress distributions in the ceramic near the interface along the *y*-direction of the cylindrical lap joint under mechanical or thermal loading.

edge and near the interface of the ceramic, respectively, on cooling from the joining temperature [2,3]. These stresses enhance the propensity to fracture of the ceramic at the edges, corners, and area adjacent to the interface [3]. Analytical and numerical calculations have revealed that regardless of the types of loading, the basic nature of stresses induced in the ceramic is the same except its magnitude [2,4,5]. Fig. 1(b) shows the stress distributions in the ceramic when the joint is under tensile stress or is cooled from bonding temperature [2,5]. Since both mechanical and thermal loading affect the same region, the lower the thermal residual stresses are, the higher the allowable stress to the fracture of the ceramic. This is the reason why, for this type of joint, the level of thermal residual stresses can characterize the mechanical strength of the joint. However, this type of analysis would not be valid, for example, in cylindrical lap joints in which a ceramic tube is constrained by a

metal shaft [6]. As can be seen in Fig. 1(c), most parts of the ceramic are highly compressed on cooling from bonding temperature, which will increase the fracture resistance of the ceramic under mechanical loading [6].

Evans et al. [3,7–11] provided theoretical background on the experimental and numerical overvations that (1) brittle fracture in the ceramic has been found to be much more likely to happen than fracture along the interface; and (2) the joint with larger thermal residual stresses fractured at lower stresses, in the same type of joints analyzed in this study [Fig. 1(a)]. They calculated the fracture resistance of a small edge crack in the ceramic and at the interface when the joint is under external loading after cooling from bonding temperature.

According to their results, large shear stress induced at the interface suppresses the crack propagation along the interface [8,10]. Under certain external load, the fracture resistance at the crack tip in the ceramic decreases as thermal residual stresses increase [11]. Compared to the effects of thermal residual stresses, stresses induced by external loading on the fracture resistance are negligible. During the mechanical test, relaxation of thermal residual stresses or modification in original residual stress distribution can occur due to the additional plastic deformation of the metal part by the applied external load. However, it only happens when the external load to fracture is many times larger than the yield stress of the metal and such high fracture strength cannot be obtained in most of ceramic-to-metal joints [11]. Therefore, brittle fracture in the ceramic at lower stress indicates that higher thermal residual stresses are induced in the ceramic-to-metal joint [3,7].

Engineers have addressed this problem by using ductile metal interlayers to relieve the residual stresses. However, single interlayers have drawbacks; for example, copper interlayers provide maximum reduction of residual stresses, but their applicability in real systems is limited due to their low resistance to corrosion and oxidation at high temperatures. To overcome the limitations of a single interlayer and for the further release of residual stresses, multiple interlayers [12–14] and functionally graded materials (FGM) have been used for some applications [15–17].

Currently, there is no deep understanding of the factors determining the residual stresses in ceramic-to-metal joints with or without interlayers because of the large number of variables involved. In addition, some experimental results seem to yield contradictory conclusions, although it is difficult to make direct comparisons in the absence of standard testing methods or requirements of size of the specimen. For example, it is not clearly understood what the most effective sequence of differing layers in multiple interlayers is, even though this type of joint has already been used in commercial products [18]. Nevertheless, theoretical study of ceramic-to-metal joints can provide a useful viewpoint for comparing the experimental results.

The purposes of this investigation are threefold:

- To develop a theoretical understanding and experimental demonstration of residual stress relief by interlayers.
- To propose improved design rules for multiple interlayers.
- To extend strain energy as a strength metric for ceramic-to-metal joints having significant plasticity.

There is no analytical model that can account for both plastic deformation and the effects of various geometries during bonding of two dissimilar materials responding to a change in temperature [4]. Numerical simulations using the finite element method (FEM) are performed in this work to analyze residual stresses from the joining process and to provide criteria for design of the interlayer prior to joining. In this study, the recoverable elastic strain energy in the ceramic has been used to measure the residual stresses as a more reliable metric of failure, as proposed by Blackwell [4].

### *1.1. Metric of failure*

For a purely elastic case, stress concentration at the periphery of the ceramic [Fig. 1(a) and (b)] has the form of a singularity ($\sigma \propto Hr^{-\lambda}$, where $\lambda$ is order of singularity and $H$ is the intensity of singularity, $r$ is a radial distance from the center of the joint) similar to the crack tip singularity in elastic frac-

ture mechanics. Contrary to the crack tip singularity, $\lambda$ is specific for each material combination and $H$ cannot be compared for material combinations of different $\lambda$ [19], which restrict singularity constants ($\lambda$ and $H$) from being used as a strength metric. The stress intensity factor ($K$) and energy release rate ($G$) at the crack tip have also been used to predict the fracture resistance of the ceramic. Since both $K$ and $G$ are dependent on the location and the size of cracks, a statistical approach to the flaw distribution in the ceramic should be used [20] and mesh formulation at the crack tip is highly restricted [7].

As mentioned previously and can be seen in Fig. 1(a) and (b), a strong stress concentration occurs along the free surface of the ceramic. The maximum tensile residual stress has been used for the strength metric most frequently. However, the maximum value of a certain component of residual stresses or strains alone cannot explain fracture behavior [8]. Fracture initiation by other components of residual stresses also cannot be ignored [7,16]. Center cracks [8] are frequently observed in cylindrical joint, which are caused by radial or circumferential stresses near the center of the joint. In addition, the presence of a singularity is problematic for FEM calculations. According to Whitcomb et al. [21], the results obtained within two elements closest to the singularity are not valid, yet this is the region where the maximum stresses are found. Although finer meshes would reduce the size of the invalid region, the peak value of stress is still inaccurate and highly mesh dependent.

Blackwell [4] addressed these problems by using strain energy in the ceramic as a metric for failure. Using FEM, Blackwell calculated the strain energy in ceramic-to-metal bonded systems without an interlayer having relatively large thickness/width ratios. Based on the fact that the strain energy in the base materials is controlled by the deformation occurring at the interface, he found that the functional dependency of the strain energy induced in the ceramic could be expressed by the following relationship:

$$U_{e,C} \sim \frac{E_C E_M^2}{(E_M + E_C)^2} \cdot (\alpha_C - \alpha_M)^2 \cdot (T - T_b)^2 \cdot (r)^3 \cdot f(h/r) \quad (1)$$

where $h$ is the height of the ceramic, $r$ is the radius of the joint and $f(h/r) \approx erf(h/r)$. $E_M$, $E_C$ are the elastic modulus of the metal and ceramic, respectively, and $\alpha_M$, $\alpha_C$ are CTE of the metal and the ceramic. $T$ is the room temperature and $T_b$ is the bonding temperature. The advantages of this approach are less dependency on the mesh formulation and rapid convergence of strain energy. The strain energy in the ceramic is calculated by summating the magnitude of $\sigma_{ij} \cdot \varepsilon_{ij} \cdot (dV)_{el}$ over all the elements in the ceramic, where $(dV)_{el}$ is the volume of each element. Since it summates the magnitude of stress over the volume of elements for which it acts, it effectively couples the magnitude of stress and its distributions [4]. Experimental results also corroborated that strain energy is a good strength metric [4,6]. Since Eq. (1) considers only the elastic behavior of materials, it cannot be applied to joints undergoing large temperature changes or those that have a significant thermal and mechanical discrepancy between the ceramic and the metal. Since plastic deformation of the metal relieves residual stresses in the joint, it is desirable to obtain general expressions of the type of Eq. (1), but which are valid in the plastic range.

The strain energy calculated from numerical modeling was summarized and generalized using the technique of order of magnitude scaling (OMS) [22], which provides simple and accurate closed form expressions based on the predominant parameters. The results obtained were verified experimentally by shear tests of $Si_3N_4$ to Inconel 718 joints with different interlayers. Experimental results showed that the simple formulations developed in this study capture the predominant factors affecting the joint strength.

## 2. Model description and experimental procedures

### 2.1. Numerical analysis

The effects of material properties on strain energy in the ceramic were investigated using a sensitivity analysis. Fictitious model materials were created for this study. For example, to investigate changes in the CTE of the interlayer, strain

energy changes were calculated for the fictitious interlayer materials that were designed to have the thermophysical properties of Ni [23] but different CTE. Similar methods were used for studying the effects of other material properties in the joint without an interlayer and joints with a single interlayer. Based on the results obtained from this sensitivity analysis, simple analytical solutions for the joints including plastic behavior of metals and metal interlayers have been developed using the OMS method.

Based on the theoretical understanding, joints with different types of multiple interlayers were modeled. As base materials, $Si_3N_4$ and Inconel 718 have been chosen. Typical types of double interlayers are laminates of a ductile material with a high CTE such as Ni and hard materials such as W having a low CTE. The strain energy in the ceramic and the stress distribution in the interlayer are compared when two layers are placed in a different order between base materials. The strain energy has also been calculated in the joint with the triple interlayer that has already been used industrially [18]. The effects of two kinds of double interlayers and one triple interlayer have been compared with Ni single interlayers with thicknesses of 0.3 and 0.9 mm. In Fig. 2, model materials and joints with single, double and triple interlayers used in numerical and/or experimental analyses have been schematically described.

To simplify the calculation as a two-dimensional problem, the specimen was modeled as a cylindrical, axisymmetric, rod-shaped specimen of 12.7 mm diameter and 12.0 mm height. The thickness of each layer in the multiple interlayers is 0.3 mm. The computational mesh is shown in Fig. 1(a). The left boundary of the mesh is the axis of symmetry. It is composed of 60–80 rows of elements along the axial direction and 30 rows of elements along the radius. The mesh was refined closer to the radial free surface and near the interface since the largest stress and strain gradients occur in these regions as shown in Fig. 1(a) [24].

The continuum models simulated cooling of a brazed specimen of $Si_3N_4$ to Inconel 718 from the bonding temperature to room temperature. Materials were assumed to be perfectly bonded at the interfaces. Uniform cooling and time-independent material properties were used. For the base metal and metallic interlayers, elastic–plastic responses were modeled. The temperature dependency of the material properties was considered [23,25]. Numerical solutions were obtained using the ABAQUS computer program [26].

### 2.2. Experimental procedure

$Si_3N_4$ was used as the ceramic material and Inconel 718 was selected for the metal. $Si_3N_4$ has been used frequently for structural components where high performance is required [27] and Inconel 718 has been used for applications in similar operational environments as $Si_3N_4$. Shear test specimens were 12.7 mm square and 10.0 mm in height for both $Si_3N_4$ and Inconel 718. For each test, five to six specimens were tested at room temperature with a constant crosshead speed of 0.5 mm/min. The test configuration is shown in Fig. 3. There is no supporting system to prevent bending of the metal, thus, the stress imposed on the interface by this test is not pure shear [28]. The peak load in the linear displacement–load curve before the actual load supported drops sharply with increasing displacement was defined as the failure load.

As interlayer materials, thin foils of Ni and W (0.3 mm) were used. Ticusil[1], brazing alloy was used in the form of thin foil ($<$0.05 mm). Prior to joining, the surfaces of the $Si_3N_4$ and the Inconel 718 were polished using SiC emery paper and diamond paste to 1 μm surface finish. All the materials were cleaned in acetone using ultrasonic vibration and dried in a warm oven. The samples were brazed at 880 °C for 20 min [29] at a vacuum pressure of $\sim 5\times10^{-6}$ Torr with a slight load of 0.5 MPa applied across the joint. The heating rate was 5~8 °C/min and the samples were furnace-cooled at 2 °C/min.

## 3. Results

### 3.1. Joints without an interlayer

Strain energy in the ceramic has been calculated for joint combinations that have been used indus-

[1] Ticusil: brazing alloy, 68.8Ag–26.7Cu–4.5wt%Ti.

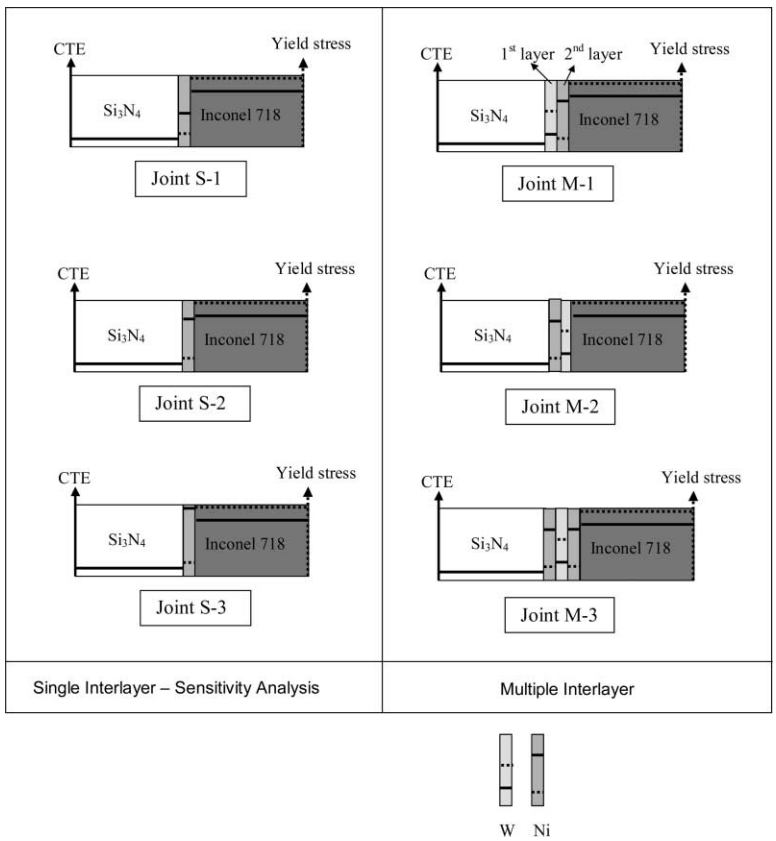


Fig. 2. A schematic of joint models.

trially and are frequently referred to in the literature (Table 1). The joint configuration used for numerical calculation was described in Section 2. As seen in Table 1, the yield stress of the metal seems to be the most important factor in reducing the strain energy in the ceramic. According to Table 1, for the same ceramic material, a metal having a higher yield stress by $x$-fold induces larger strain energy by nearly $x^2$. Alternatively, other parameters such as the difference in elastic modulus and CTE seem to be not as important as the yield stress of the metal.

As described in Section 2, a sensitivity analysis was performed on the $Si_3N_4$–Ni joint in Table 1 to investigate the effect of various parameters on strain energy development in the ceramic. As expected from previous calculations of strain energy (Table 1), it has been confirmed that strain energy changes induced by varying material properties are negligible compared to those produced due to changes in the yield stress of the metal. Increasing the radius and the $h/r$ ratio, however, is not negligible. With regard to the strain energy changes changing the radius and $h/r$ ratio, similar functional relationships as with the elastic case [Eq. (1)] have been obtained; the strain energy is proportional to the radius cubed and the effect of $h/r$ becomes negligible if the value of $h/r$ is greater than one, although the strain energy increases rapidly with the ratio $h/r$ smaller than one.

### *3.1.1. Analytical expression*

To obtain an analytical expression, we used OMS [22], which provides closed-form expressions for systems with simultaneous driving forces. Based on our sensitivity analysis using FEM calculations, a scaling factor for the strain

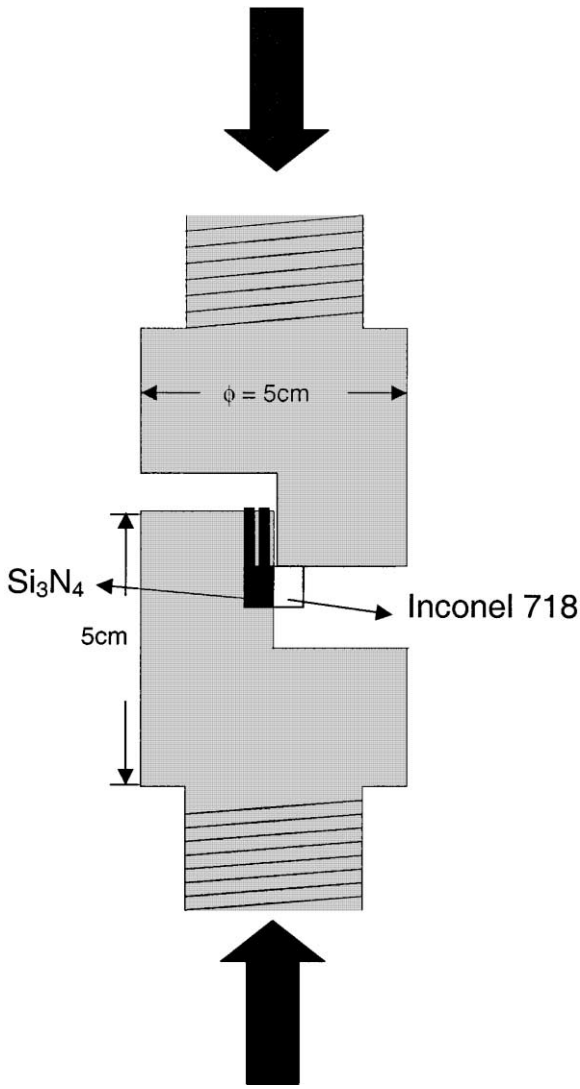


Fig. 3. A schematic description of shear test configuration.

energy in the ceramic was obtained, and the most relevant dimensionless group was identified.

The strain energy in the ceramic is calculated as

$$U_{e,C} = \int \frac{1}{2}\sigma_{ij}\varepsilon_{ij}(dV)_{el}. \quad (2)$$

The integral of Eq. (2) can be estimated as

$$U_{e,C} \approx \hat{U}_{e,C} = \sigma_c \varepsilon_c V_c \quad (3)$$

where $\varepsilon_c$ and $\sigma_c$ are the characteristic strain and stress in the ceramic, and $V_c$ is the characteristic volume over which the stress and strain are produced. Since the ceramic behaves elastically, $\varepsilon_c = \sigma_c/E_C$. Numerical simulations indicate that the characteristic volume is of the order of $r^3$; thus, the elastic energy stored in the ceramic can be estimated as:

$$\hat{U}_{e,C} = \frac{\sigma_c^2 r^3}{E_C}. \quad (4)$$

The characteristic stress in the ceramic depends on the amount of plasticity in the metal. In the asymptotic case when all the metal near the joint is in the plastic regime, the characteristic stress in the ceramic is given by the yield stress of the metal: $\sigma_c = \sigma_{YM}$. When some of the metal is not in the plastic regime, Eq. (4) must be corrected. In this case, the dimensionless group that captures the effect of partial plasticity is the ratio of the residual strain at the interface and the yield strain of the metal:

$$\Pi = \frac{(\alpha_M - \alpha_C)\Delta T E_M}{\sigma_{YM}} \quad (5)$$

where $\sigma_{YM}$ is the yield stress of the metal at room temperature. Based on Eqs. (4) and (5), the strain energy in the ceramic can be calculated as:

$$U_{e,C} = \frac{\sigma_{YM}^2 r^3}{E_C} f(\Pi). \quad (6)$$

The correction function $f(\Pi)$ does not include the geometry parameter $h/r$ because it is intended for joints having relatively large thickness. This function can be determined by analyzing FEM calculations of strain energy in the ceramic (Table 1). For values of $\Pi$ larger than 0.5 the following expression of $f(\Pi)$ provides values of strain energy within 10% of the numerical calculations, as shown in Fig. 4:

$$f(\Pi) = 0.035\Pi + 0.563. \quad (7)$$

### 3.2. Joints with a single interlayer

It is known that metal interlayers with low yield stress reduce the strain energy in the base materials

Table 1
Strain energy in the selected joint systems without an interlayer

| Ceramic–metal | $\alpha_M-\alpha_C$ ($\times10^{-6}$/°C) | $E_C-E_M$ (GPa) | $\sigma_{YM}$ (MPa) | $U_{e,C}$ ($\times10^{-3}$, J) |
|---|---|---|---|---|
| $Si_3N_4$–Cu | 13.7 | 176 | 75.8 | 4.23 |
| $Si_3N_4$–Ni | 10.3 | 96 | 148 | 15.2 |
| $Si_3N_4$–Nb | 4.2 | 201 | 240 | 25.9 |
| $Si_3N_4$–Inconel 600 | 10.3 | 98 | 250 | 37.8 |
| $Si_3N_4$–304SS | 14.2 | 104 | 255.5 | 38.8 |
| $Si_3N_4$–AISI 316 | 14 | 110 | 289.6 | 49.1 |
| $Al_2O_3$–Ti | 1.01 | 238 | 172 | 10.4 |
| $Al_2O_3$–Inconel600 | 5.9 | 152 | 250 | 30.0 |
| $Al_2O_3$–304SS | 9.8 | 158 | 255.5 | 31.6 |

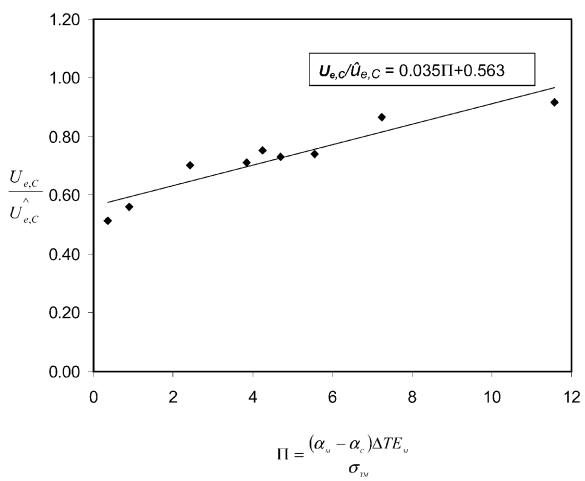


Fig. 4. Normalized strain energy as a function of normalized thermal strain.

[17,24,30,31]. FEM investigations by Williamson et al. [24] showed the important trade-off between residual stress relief in the ceramic and increasing plastic deformation in the interlayer. As in Section 3.1, OMS has been used for obtaining a closed form expression for the strain energy in the ceramic. In this case, the characteristic stress in the ceramic is given by the yield strength of the interlayer $\sigma_{YI}$.

Since the interlayer adds a new degree of freedom to the system, the correction function will depend on two parameters instead of one as before. To determine this additional parameter, a sensitivity analysis was performed.

### *3.2.1. Effect of interlayer material properties on stress relief in the ceramic*

For the selected joint systems, strain energy has been calculated and the results are summarized in Table 2. The selected joint systems have a relatively large CTE difference between base materials. Intensive research has investigated the effect of interlayers with intermediate CTE between the ceramic and that of the metal; however, materials with smaller CTE generally have a high yield stress. Based on the numerical analysis results, the interlayers with a yield stress higher than that of the metal induce even larger strain energy than when an interlayer is not used. Therefore, joints with an interlayer of intermediate CTE but a higher yield stress than that of the metal have been excluded in this work.

In order to examine the effects of interlayer material properties other than the yield stress, sensitivity analysis has been done with one of the selected joint systems ($Si_3N_4$–Ni–Inconel 718 joint in Table 2). Strain energy changes were calculated for fictitious interlayer materials that were designed to have the thermophysical properties of Ni but a different CTE. Similar methods were used for studying the effects of other interlayer material properties such as elastic modulus, the degree of hardening and the thickness of the interlayer ($t$). In terms of practical applications, a thinner interlayer is generally better. In this study, the range of the interlayer thickness of interest lay between 0.3 and 2 mm, which is 1/40 and 1/6 of the height of the base material, respectively. It was found that

Table 2
Strain energy in the selected joint systems with a single interlayer

| Ceramic–interlayer–metal | $\sigma_{YM}$ (MPa) | $\sigma_{YI}$ (MPa) | $\alpha_M-\alpha_C$ ($\times10^{-6}$/°C) | $U_{e,C}$ ($\times10^{-3}$, J) |
|---|---|---|---|---|
| $Si_3N_4$-Cu-In600 | 250 | 75.8 | 10.3 | 3.60 |
| $Si_3N_4$-Cu-304SS | 255.5 | 75.8 | 14.2 | 4.15 |
| $Si_3N_4$-Cu-Inc718 | 1036 | 75.8 | 10.3 | 3.65 |
| $Si_3N_4$-Ti-In600 | 250 | 172 | 10.3 | 18.2 |
| $Si_3N_4$-Ti-304ss | 255.5 | 172 | 14.2 | 18.5 |
| $Si_3N_4$-Ti-AISI316 | 289.6 | 172 | 14 | 18.5 |
| $Si_3N_4$–Ni–Ti | 172 | 148 | 5.41 | 11.5 |
| $Si_3N_4$–Ni–In600 | 250 | 148 | 10.3 | 14.8 |
| $Si_3N_4$–Ni–304SS | 255.5 | 148 | 14.2 | 16.5 |
| $Si_3N_4$–Ni–Inc718 | 1036 | 148 | 10.3 | 15.0 |
| $Si_3N_4$–Nb–In600 | 250 | 240 | 10.3 | 34.5 |
| $Si_3N_4$–Nb–304SS | 255.5 | 240 | 14.2 | 35.5 |
| $Si_3N_4$–Nb– Inc718 | 1036 | 240 | 10.3 | 33.1 |
| $Si_3N_4$–Mo–Inc718 | 1036 | 370 | 10.3 | 74.4 |
| $Al_2O_3$–Cu–In600 | 250 | 75.8 | 5.9 | 2.56 |
| $Al_2O_3$–Cu–304SS | 255.5 | 75.8 | 9.8 | 3.23 |
| $Al_2O_3$–Cu–In718 | 1036 | 75.8 | 5.9 | 4.18 |
| $Al_2O_3$–Ni–In600 | 250 | 148 | 5.9 | 11.5 |

changes in properties of the interlayer other than CTE do not significantly affect the strain energy in the ceramic. As in joints without an interlayer, FEM calculations showed that the strain energy in the ceramic is proportional to the radius cubed and the effect of the $h/r$ ratio is negligible when it is over one.

The strain energy change in the ceramic ($U_{e,C}$) and plastic strain energy change in the interlayer ($U_{p,I}$) as a function of CTE are shown in Fig. 5. Since a ductile interlayer with a smaller CTE than the ceramic is physically unrealistic, the minimum CTE evaluated was limited to values larger than $\alpha_{Si3N4}$ (=3.0×$10^{-6}$/°C). In Fig. 5, as CTE of the interlayer, $\alpha_I$, becomes larger than $\alpha_M$, (1) less strain energy is induced in the ceramic and (2) larger plastic strain energy dissipation occurs in the interlayer. Based on these results, a new parameter $\Phi$ is proposed.

$$\Phi = 1-\left(\frac{\alpha_M-\alpha_I}{\alpha_C-\alpha_I}\right)^m \quad (8)$$

where $m = 1$ when $\alpha_I$ is larger than $(\alpha_M + \alpha_C)/2$ and $m = -1$ for $\alpha_I$ values smaller than $(\alpha_M + \alpha_C)/2$. Assuming that a value of $\Phi$ closer to zero indicates less strain energy induced in the ceramic, the parameter shows that (1) as $\alpha_I$ becomes much larger even than $\alpha_M$, less strain energy will be induced in the ceramic, and (2) for otherwise identical interlayers, less strain energy is induced in the ceramic, as $(\alpha_M-\alpha_C)$ decreases.

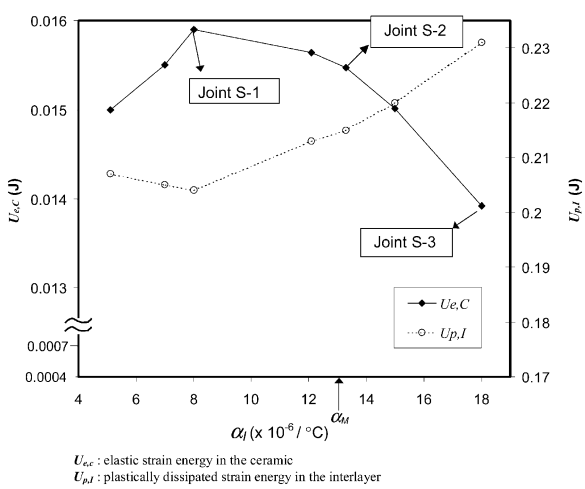


Fig. 5. Elastic strain energy in the ceramic and plastic strain energy in the interlayer as a function of CTE of the interlayer.

*3.2.2. Analytical expression*

As in Section 3.1, a scaling factor for the strain energy in the ceramic and the most relevant dimensionless group can be identified, based on sensitivity analysis. As in the case of joints without an interlayer, the dimensionless group that captures the effect of partial plasticity at the interface was defined as the ratio of residual strain at the interface and yield strain of the interlayer, $\Pi_I$. The new parameter, $\Phi$, captures the effect of having three independent CTEs in a system with one interlayer. The relative differences in CTEs of three materials (the metal, the ceramic and the interlayer) also affect the plastic deformation in the entire volume of the interlayer and thus, the strain energy in the ceramic (in Fig. 5). This effect has been captured by the parameter, $\Phi$, in the previous sensitivity analysis. Therefore, the correction function includes two dimensionless groups: $\Pi_I$ and $\Phi$. The scaling factor and two dimensionless groups are defined as follows:

$$U_{e,C} = \frac{\sigma_{YI}^2 r^3}{E_C} f(\Pi_I, \Phi) \tag{9}$$

$$\Pi_I = \frac{(\alpha_M - \alpha_C)\Delta T E_I}{\sigma_{YI}} \tag{10}$$

$$\Phi = 1 - \left(\frac{\alpha_M - \alpha_I}{\alpha_C - \alpha_I}\right)^m.$$

The correction function can be validated by analyzing FEM calculations of strain energy in the ceramic of the selected joint systems as shown in Table 2. For values of $\Pi_I$ larger than two and $\Phi$ larger than 0.5, the following function of $\Pi_I$ and $\Phi$ provides values of strain energy in the ceramic within 10% of the numerical calculations:

$$f(\Pi_I, \Phi) = 0.027\Pi_I + 0.110\Phi + 0.491. \tag{11}$$

As mentioned previously, it is known that there is a trade-off between the residual stresses in the ceramic and plastic deformation of the interlayer. Since three independent CTEs in a system will change the stress and strain distribution in the interlayer, the accommodation of strain energy in the ceramic with variation in $\Phi$ has been investigated in terms of the effect of these changes on plastic deformation in the interlayer.

*3.2.3. Stress distribution in the interlayer and its effect on stress relief in the ceramic*

The two largest components of residual stresses in the interlayer are $\sigma_{xx}$ and $\sigma_{xy}$. Since the lateral deformation of the interlayer is highly constrained by adhesion with the ceramic, the shear stress, $\sigma_{xy}$, is generally larger than $\sigma_{xy}$ near the interface. In addition, as $(\alpha_M - \alpha_C)$ increases, $\sigma_{xx}$ tends to remain stable, while $\sigma_{xy}$ increases significantly [31].

The residual stress distributions in the interlayer have been analyzed and compared for the three fictitious joint systems described in Figs. 2 and 5. In joint S-1, the CTE of the Ni interlayer has been modified as $\alpha_{Inconel718} + \alpha_{Si_3N_4}/2$, and in joint S-3, it is $18\times10^{-6}$/°C ($>\alpha_{Inconel\ 718}$). Joint S-1 has the largest values of $\Phi$ whereas joint system S-3 has the smallest. The distribution of $\sigma_{xx}$, $\sigma_{xy}$, $\sigma_{yy}$ along the interface in the three joints are compared in Fig. 6. As seen in Fig. 6, the change in tensile stress, $\sigma_{yy}$, with $\Phi$ is negligible compared to the changes in the other two components. Closer to the free edge, both $\sigma_{xx}$ and $\sigma_{yy}$ increase rapidly, which will result in larger plastic deformation near the free edge. As $\Phi$ becomes smaller, $\sigma_{xx}$ increases faster than does $\sigma_{xy}$ and the distribution of $\sigma_{xx}$ becomes more uniform through the thickness of the interlayer as seen in Fig. 7(a). Alternatively, the distribution of $\sigma_{xy}$ through the interlayer [Fig. 7(b)] becomes more symmetric as $\Phi$ becomes smaller, which induces less stress in base materials. The distributions of these two stress components in the interlayer of joints S-1 and S-3 are shown schematically in Fig. 8 with the contours of plastic strain energy density in the interlayer. Fig. 8(a) shows that stress distributions with large gradients result in much larger residual elastic strain remaining in the interlayer of joint S-1, which induces more strain energy in the ceramic, as in Fig. 5. The more uniform and more symmetric distributions of $\sigma_{xx}$ and $\sigma_{xy}$ in joint S-3 cause less bending in the interlayer and cause plastic deformation to occur over a larger volume of the interlayer as seen in Fig. 8(b). This induces less strain energy in the ceramic as shown in Fig. 5.

As the relative CTE difference between the base materials and the interlayer $(\alpha_M - \alpha_I/\alpha_C - \alpha_I)^m$ approaches one [i.e. $\Phi = 1 - (\alpha_M - \alpha_I/\alpha_C - \alpha_I)^m$ is

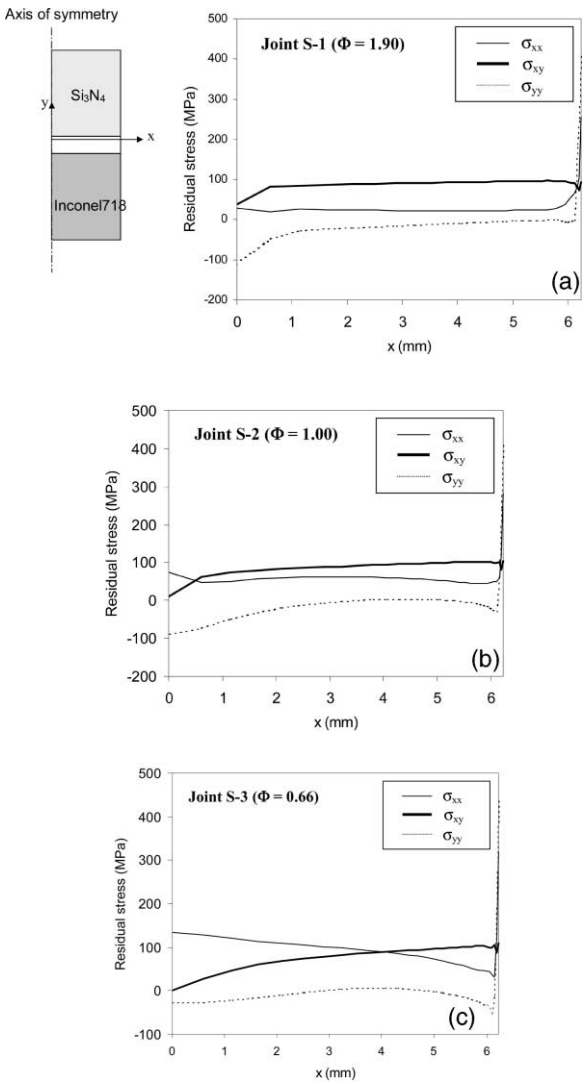


Fig. 6. Residual stress distributions in the interlayer near the interface along the *x*-direction: (a) joint S-1, (b) joint S-2, (c) joint S-3.

close to zero), (1) the stress state develops into one where more than one stress component dominates, and (2) the distribution becomes more uniform and symmetric, which facilitates yielding of the interlayer over the entire volume as well as near the interface.

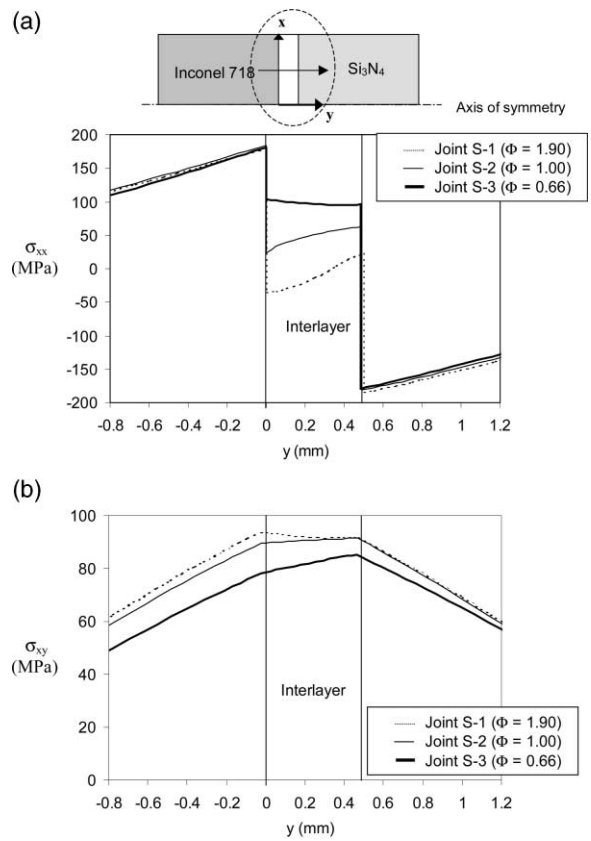


Fig. 7. Residual stress distributions along the *y*-direction in the interlayer of joints S-1, S-2, and S-3: (a) $\sigma_{xx}$, (b) $\sigma_{xy}$.

### 3.3. Design of multiple interlayers

Based on the results obtained in cases with single interlayers, the two types of double interlayers that have been described in Fig. 2 can be evaluated in two aspects: (1) the yield stress of the layer next to the ceramic and (2) the CTE gradient from the ceramic to the metal. According to the previous results, the yield stress of the interlayer is the most important parameter affecting the strain energy in the ceramic. However, tailoring the CTE gradient from the ceramic to the metal represented by $\Phi$ is also an important parameter to relieve the strain energy.

In joint M-1 in Fig. 2, the CTE of the first layer next to the ceramic is closer to the CTE of the ceramic, which may mitigate residual stresses due to the abrupt increase in CTE between the ceramic

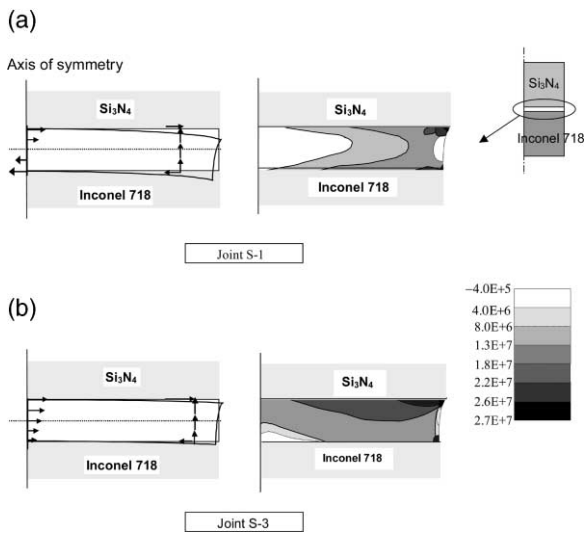


Fig. 8. A schematic description of stress distribution and the contour of plastic strain energy in the interlayer of (a) joint S-1 and (b) joint S-3.

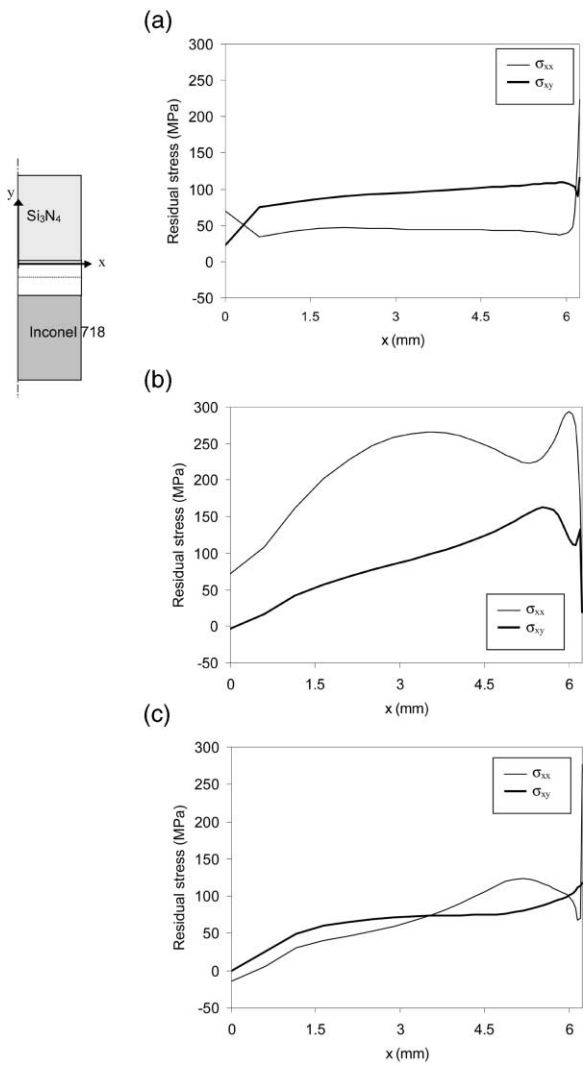


Fig. 9. Residual stress distribution in the interlayer near the interface with the ceramic: (a) joint with 0.3 mm Ni single interlayer; (b) joint M-1: $Si_3N_4$/0.3 mm W/0.3 mm Ni/Inconel 718; (c) joint M-2: $Si_3N_4$/0.3 mm Ni/0.3 mm W/Inconel 718.

and the ductile second layer or the metal. However, the yield stress of the first layer is higher than that of the ductile layer placed next to the ceramic in joint M-2 (or the joint with a single Ni interlayer), which may limit the release of residual stresses. If one assumes that the first and second layer in joints M-1 and M-2 have similar mechanical properties but different CTEs, the parameter $\Phi$ is another parameter to determine the most effective sequence of layers in the double interlayer. When the CTE of a second layer [$\alpha_{I(2)}$] inserted between the metal and the first layer is used instead of $\alpha_M$ in Eq. (8), joint M-2 in Fig. 2 has a value $\Phi = 0.15$ which is closer to zero than the value of $\Phi = 1.17$ of joint M-1, in which the CTE decreases when moving from the metal to the ceramic. As the difference between $\alpha_{I(2)}$ and $\alpha_C$ decreases, $\Phi$ becomes closer to zero, which should improve the stress distribution in the interlayer, thus producing less strain energy in the ceramic.

In Fig. 9, distributions of the major stress components $\sigma_{xx}$ and $\sigma_{xy}$ near the interface between the first layer and the ceramic of joints M-1 and M-2 have been compared with those in the joint with a single interlayer of 0.3 mm Ni. Although the CTE difference between the ceramic and the first interlayer is smaller in joint M-1, larger stresses have been induced in the interlayer due to the high yield stress of the tungsten. In addition to the high yield stress, placing layers in order of increasing CTE as compared with the ceramic causes quite a different stress state in the first layer of joint M-1 from in the joints with either a single interlayer or joint M-2. As seen in Figs. 9(b) and 10(a), $\sigma_{xx}$ is the largest stress component in the first layer of joint M-1 and its gradient through the

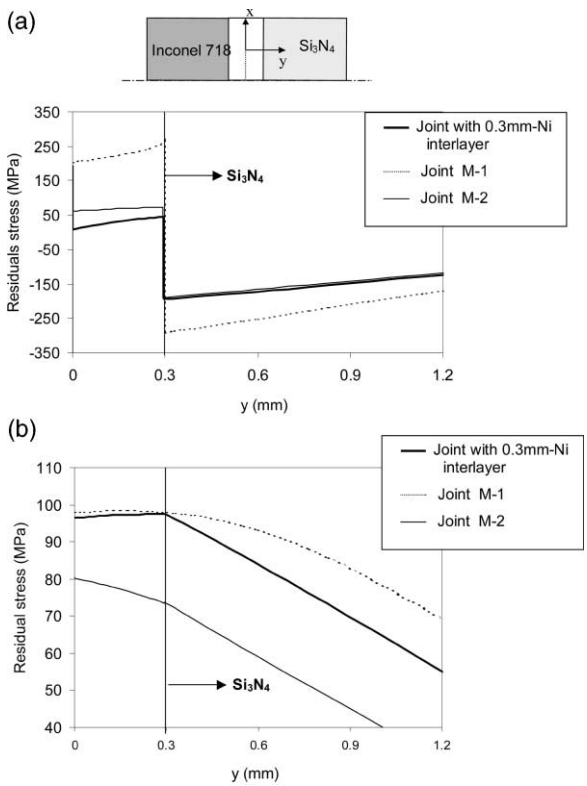


Fig. 10. Residual stress distributions through the interlayer thickness: (a) $\sigma_{xx}$, (b) $\sigma_{xy}$.

interlayer is the largest among the joints being compared, thus inducing a larger tensile residual stress in the ceramic. The distribution of $\sigma_{xy}$ through the layer becomes less symmetric than in the joint with a single interlayer. In contrast, in joint M-2, $\sigma_{xx}$ in the first ductile layer has been increased by inserting an additional hard layer having a lower CTE than the first layer; however, the magnitudes of $\sigma_{xx}$ and $\sigma_{xy}$ are comparable as shown in Fig. 9(c). Compared to the stress state in the single 0.3 mm Ni interlayer, $\sigma_{xx}$ increased uniformly through the layer as shown in Fig. 10(a) and $\sigma_{xy}$ has become more symmetric as shown in Fig. 10(b), which leads to less residual stress in the ceramic.

As mentioned previously, joint M-1 with a larger $\Phi$ shows that $\sigma_{xx}$ is the largest stress component and its distributions with a large gradient through the layer seem to create greater bending in this layer. Such stress distributions resulted from high yield stresses in the first layer and the large $\Phi$ of joint M-1 have induced larger strain energy in the ceramic than the single 0.3 mm Ni interlayer shown in Table 3. Alternatively, lower yield stress of the first layer and the order of placement producing smaller values of $\Phi$ in joint M-2, make plastic deformation occur over a larger volume of the first ductile layer and induce less strain energy in the ceramic than in the joint with a 0.3 mm Ni interlayer. This indicates that the additional hard layer having a lower CTE in joint M-2 improves the function of the ductile interlayer by modifying the stress distributions in the interlayer. The relationship between changes in stress distributions in the first layer by addition of more interlayers and changes in the strain energy in the ceramic show similar results as those obtained by changing the CTE of the single interlayer in Section 3.2.

With the triple interlayer in joint M-3 (Fig. 2), plastic deformation of a third ductile interlayer between the second interlayer and the metal will further reduce the effect of the metal on the stress distribution in the first ductile interlayer, and hence will further reduce the strain energy in the ceramic. Calculation results in Table 3 indicate that a great deal of strain energy in the second interlayer [$U_{e,I(2)}$, $U_{p,I(2)}$] has been reduced in joint M-3 in contrast to joint M-2 due to the considerable plastic deformation in the third ductile layer in joint M-3. Compared to the joint with a single ductile interlayer of the same thickness (0.9 mm), more strain energy is relieved in joint M-3 with the triple interlayer of 0.3 mm per layer (Table 3).

### 3.4. Experimental validation

Shear test specimens were prepared following the procedures described in Section 2.2, and the test results are shown in Table 4 with specimen configuration. The test specimen without an interlayer (specimen 1) fractured under the lowest load. The degree of scatter in the measured strength values was also large. The average strength of the joints with the double interlayer of increasing CTE from the ceramic (specimen 4) was lower than that of joints with a single Ni interlayer and only slightly higher than that of the joint without an interlayer. The joints with an additional hard inter-

Table 3
Strain energy in six model joints[a]

| | $U_{e,C}$ ($\times 10^{-2}$, J) | $U_{e,M}$ ($\times 10^{-2}$, J) | $U_{e,I(1)}$ ($\times 10^{-2}$, J) | $U_{p,I(1)}$ (J) | $U_{e,I(2)}$ ($\times 10^{-2}$, J) | $U_{p,I(2)}$ (J) | $U_{e,I(3)}$ ($\times 10^{-2}$, J) | $U_{p,I(3)}$ (J) |
|---|---|---|---|---|---|---|---|---|
| Joint without an interlayer | 4.511 | 5.896 | – | – | – | – | – | – |
| Joint with 0.3 mm Ni | 1.650 | 2.116 | 2.435 | 0.221 | – | – | – | – |
| Joint M-1 | 2.314 | 1.798 | 3.872 | 0.0001 | 2.394 | 0.206 | – | – |
| Joint M-2 | 1.304 | 2.514 | 0.243 | 0.103 | 1.685 | 0.015 | – | – |
| Joint M-3 | 1.101 | 1.914 | 0.258 | 0.081 | 0.967 | 0.002 | 0.224 | 0.115 |
| Joint with 0.9 mm Ni | 1.570 | 1.480 | 0.480 | 0.222 | – | – | – | – |

[a] $U_{e,M}$, elastic strain energy in the metal; $U_{e,I(1)}$, elastic strain energy in the first interlayer; $U_{p,I(1)}$, plastic strain energy in the first interlayer; $U_{e,I(2)}$, elastic strain energy in the second interlayer; $U_{p,I(2)}$, plastic strain energy in the second interlayer; $U_{e,I(3)}$, elastic strain energy in the third interlayer; $U_{p,I(3)}$, plastic strain energy in the third interlayer.

Table 4
Specimen configuration and test results

| | |
|---|---|
| Specimen 1 | $Si_3N_4$/Inconel 718 |
| Specimen 2 | $Si_3N_4$/0.3 mm Ni/Inconel 718 |
| Specimen 3 | $Si_3N_4$/0.3 mm Ni/0.3 mm W/Inconel 718 |
| Specimen 4 | $Si_3N_4$/0.3 mm W/0.3 mm Ni/Inconel 718 |
| Specimen 5 | $Si_3N_4$/0.3 mm Ni/0.3 mm W/0.3 mm Ni/Inconel 718 |

| | Minimum (MPa) | Average (MPa) | Maximum (MPa) |
|---|---|---|---|
| Specimen 1 | 1.5 | 17.0 | 36.2 |
| Specimen 2 | 10.0 | 32.0 | 48.0 |
| Specimen 3 | 24.8 | 59.0 | 62 |
| Specimen 4 | 18.24 | 21.0 | 25 |
| Specimen 5 | 49.6 | 62.0 | 80.6 |

layer next to the ductile interlayer (specimen 3) showed a nearly 30% increase in the average strength compared to joints with a single interlayer; however, the maximum strength of specimen 3 is nearly the same as the joints with 0.3 mm Ni interlayer. The large difference in strength of the two double interlayer models (specimens 3 and 4) indicates the importance of interlayer sequence when using multiple interlayers.

As seen in Table 3, by inserting a third ductile interlayer, the strain energy in the ceramic of specimen 5 is reduced by 40% as compared to specimen 2 with a single interlayer. The maximum strength of these joints is increased by 35% compared to joints with a single interlayer and the average strength was increased almost 100%. Overall, the joint having a 0.9 mm triple interlayer has the highest average strength and it has the lowest calculated strain energy. Comparing the strength data in Table 4 with the strain energy calculation in Table 3, the test results are consistent with FEM calculations of the strain energy in the ceramic in that joints with less strain energy in the ceramic show higher strength. Fig. 11 shows the relationship between the strength and strain energy of the ceramic in each joint. The plot indicates that the strength of the joint increases with decreasing strain energy in the ceramic, which suggests that the strain energy in the ceramic is a reliable metric for joint strength.

Except for a few joints having no interlayer, the

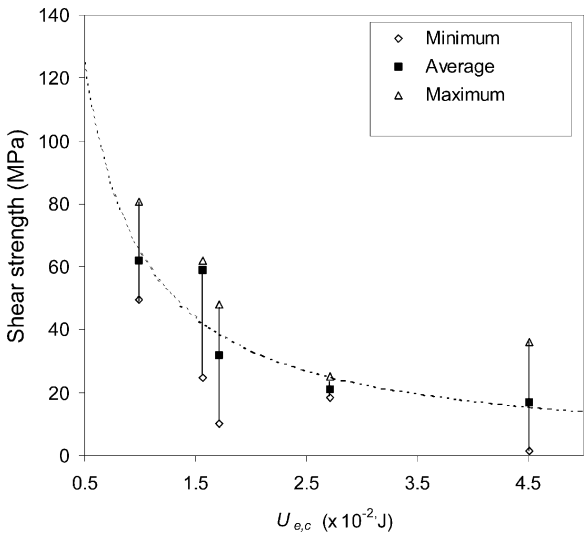


Fig. 11. Shear strength vs. calculated strain energy in the ceramic.

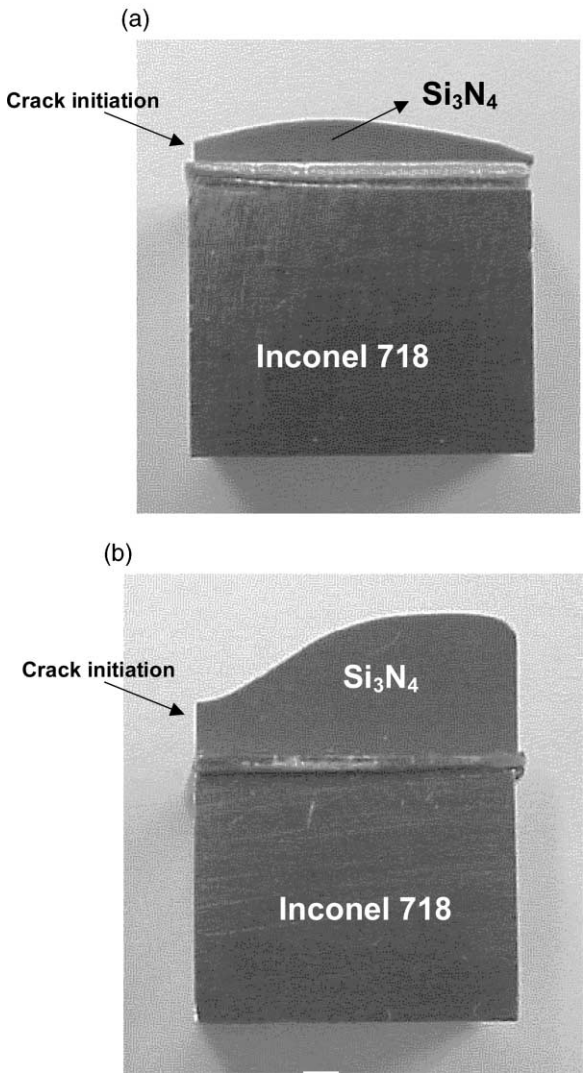


Fig. 12. Different fracture patterns of joints with (a) relatively low strength, (b) higher strength.

crack initiated in the ceramic adjacent to the interface, propagated and ended in the ceramic. In joints with interlayers, no brittle interfacial fractures were observed. Two different types of fractured specimens after the test are shown in Fig. 12. In the fracture shown in Fig. 12(a), the crack initiated very close to the interface and propagated in the ceramic with a concave shape. This is typical of fractures in joints with large thermal expansion mismatch and low strength [28]. In joints with greater strength, fracture occurs as shown in Fig. 12(b). The crack path is well removed from the ceramic interface, thus increasing the strength of the joint.

## 4. Discussion

It can be argued that a compressive triaxial state of stress would make a joint stronger while the strain energy also increases. This would make the proper use of strain energy as a joint strength metric dependent on the geometry of the problem. In our system only a small portion of the volume along the center of the axis is in this state as seen in Fig. 1(a). The smaller the compressive strain at the interface of the ceramic and the smaller the $h/r$ ratio, the lower the triaxial compressive state of stress induced, and the volume where it occurs decreases. The volume over which the triaxial state of stress occurs may affect the fracture path. However, according to our FEM calculations, the magnitude of the strain energy calculated over the volume of triaxial compressive stress is negligible (less than 15%) compared to the total strain energy in the ceramic. This small value supports the use of strain energy as an appropriate strength metric.

This conclusion is also validated by the experimental results summarized in Fig. 11.

Based on the FEM calculations for multiple interlayers, it appears that properly designed multiple interlayers can reduce the strain energy in the ceramic more effectively than a single interlayer; however, the most desirable gradation of interlayer properties is not a simple linear decrease from one base material to the other. Use of rigid layers with increasing CTE away from the ceramic interface and insertion of ductile layers between each rigid layer will reduce the strain energy most effectively. As an example, in Table 3, the triple interlayer accommodates more strain energy than a single ductile interlayer of the same thickness (0.9 mm). However, a multiple interlayer is not always desirable in practice. A larger number of layers requires more joint interfaces and the probability of producing defects will increase with the number of interfaces. This can be the cause of failure even at very low stresses.

The relative thickness ratio of each layer in the multiple interlayer affects the strain energy distribution in the joint. Suganuma et al. investigated the effect of the thickness of second interlayers [13]. For a system similar to joint M-2, they found an optimum thickness of the second interlayer in minimizing the strain energy in the ceramic. Our rule of design for multiple interlayers could be enhanced by considering these effects.

## 5. Conclusions

A multiple interlayer design rule has been proposed based on closed form functional relationships between material properties and strain energy developed for ceramic-to-metal joints with a single interlayer [Eqs. (8)–(11)]. The simple analytical expressions indicate that strain energy in the ceramic scales with the square of the yield stress of an interlayer. In addition, two factors were found to affect the relationships: the CTE difference between the ceramic and the metal (captured by parameter $\Pi_1$), and the relative CTE difference between the ceramic, the metal, and the interlayer (captured by parameter $\Phi$). The parameter $\Phi$ [Eq. (8)] quantifies the uniformity and symmetry of the residual stress distribution through the interlayer due to the CTE mismatch between the materials involved in the joint. As $\Phi$ becomes closer to zero, the stress distribution in the interlayer has a smaller gradient and becomes more symmetric, which causes a larger volume of the interlayer to deform plastically. This more homogeneous stress distribution causes a reduction of the strain energy in the ceramic due to the joining process, thus strengthening the joint.

Although the CTE of the interlayer material cannot be controlled easily, use of multiple interlayers can create even greater reductions in strain energy by redistributing the stress and plastic strain in a ductile interlayer next to the ceramic. The analytical model and numerical results indicate that inserting an additional rigid layer with lower CTE next to the ceramic to mitigate large differences in CTE between the ceramic and the ductile interlayer induces more strain energy than the single ductile interlayer, which results from the larger yield stress of the rigid layer and less symmetric stress distribution in the interlayer. In contrast, a rigid interlayer with a low CTE can enhance the beneficial effect of the ductile interlayer when it is inserted between the metal and the ductile interlayer. Further decreases in strain energy of the ceramic can be achieved with a third ductile interlayer by reducing the residual strain induced in the second rigid interlayer due to mismatch with the metal.

Our experiments confirm the proposed design rules for multiple interlayers and that the strain energy in the ceramic is a good strength metric for ceramic-to-metal joints. For example, joints with an appropriately designed triple interlayer showed the minimum strain energy in our FEM calculations, and the highest strength of all joints tested. This supports the use of strain energy as a joint strength metric.

## Acknowledgement

This research was funded under the United States DOE Award No. DE-FC26-99FT400054.

## References


[1] Schwartz MM. Ceramic joining. Materials Park (OH): ASM International, 1990.
[2] Evans AG, Ruhle M, Turwitt M. J de Physique 1980;c4:C4.
[3] He MY, Evans AG. Acta metall 1991;39:1587.
[4] Blackwell BE. PhD thesis, Department of Material Science and Engineering, MIT; 1996.
[5] Park J-W, Eagar TW. In preparation.
[6] Wiese JL, Park J-W, Eagar TW. Scripta mater, submitted for publication.
[7] Cao HC, Thouless MD, Evans AG. Acta metall 1988;36:2037.
[8] Bartlett A, Evans AG, Ruhle M. Acta metall 1991;39:1579.
[9] Dalgleish BJ, Lu MC, Evans AG. Acta metall 1988;36:2029.
[10] Evans AG. Acta metall 1989;37:3249.
[11] Hsueh CH, Evans AG. J Am Ceram Soc 1985;68:241.
[12] Hao H. J Mater Sci 1995;30:4107.
[13] Suganuma K, Okamoto TM. Comm Am Ceram Soc 1984;C-256.
[14] Xian A-P, Si Z-Y. J Mater Sci 1992;27:1560.
[15] Drake JT, Williamson RL. J Appl Phys 1993;74:1321.
[16] Williamson RL, Rabin BH. J Appl Phys 1993;74:1310.
[17] Rabin BH, Williamson RL, Suresh S. MRS Bull 1995;37.
[18] Foley AG. Industrial Ceram 1999;19:193.
[19] Akisanya AR. J Strain Analysis 1997;32:301.
[20] Selverian JH, O'Neil D, Kang S. Am Ceram Soc Bull 1992;71:1403.
[21] Whitcomb JD, Raju IS, Goree JG. Comps Struct 1982;15:23.
[22] Mendez P. PhD thesis, Department of Material Science and Engineering, MIT; 1999.
[23] Metals handbook. 2nd ed. Materials Park (OH): ASM International, 1998.
[24] Williamson RL, Rabin BH, Byerly GE. Composites Eng 1995;5:851.
[25] ABAQUS/theory manual ver. 6.1. HKS; 2000.
[26] ABAQUS ver. 6.1-2. HKS.
[27] Peteves SD. JOM 1996;48.
[28] Nicholas MG, editor. Joining of ceramics. Adv. Ceram. Rev., Chapman and Hall; 1990.
[29] Zhuang W-D. PhD thesis, Department of Material Science and Engineering, MIT; 1996.
[30] Travessa DN, Ferrante M. Mater Sci Tech 2000;16:687.
[31] Xian A-P, Si Z-Y. J Am Ceram Soc 1990;73:3462.